Supplementary Information

Hydrogen-Bonded MXene Ohmic Contacts: Overcoming Schottky and Tunneling Barriers for Quantum-Limit 2D-MoS_2 Electronics

Weishu Chen[#], Tao Shen[#], Ji-Chang Ren[*] and Shuang Li[*]

[a] Nano and Heterogeneous Materials Center, School of Materials Science and Engineering, Nanjing University of Science and Technology, Nanjing 210094, China.

[#] These authors contributed equally to this work.

Figure S1. (**a**) The projected band and density of states (DOS) diagrams for $Ta_3C_2O_2$ and (**b**) Ta_3C_2 heterostructures with MoS_2 under M-S stacking, where the gray scattered points in the projected band diagram represent the energy bands of the entire heterostructure, the red scattered points represent the energy bands of MoS_2, the distance between the blue horizontal line and the Fermi level corresponds to the Schottky barrier (Φ_{SB}). The Fermi level is set at 0 eV, and 'Total' in the DOS diagram represents the entire heterostructure.

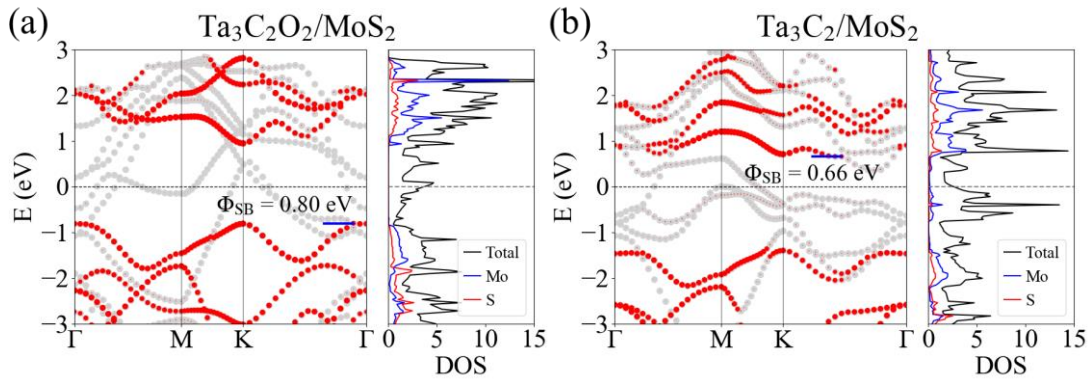

Figure S2. Projected band and DOS diagrams for the six types of $M_3C_2(OH)_2/MoS_2$ with three different stacking modes, with the corresponding parameters having the same meaning as in Figure S1.

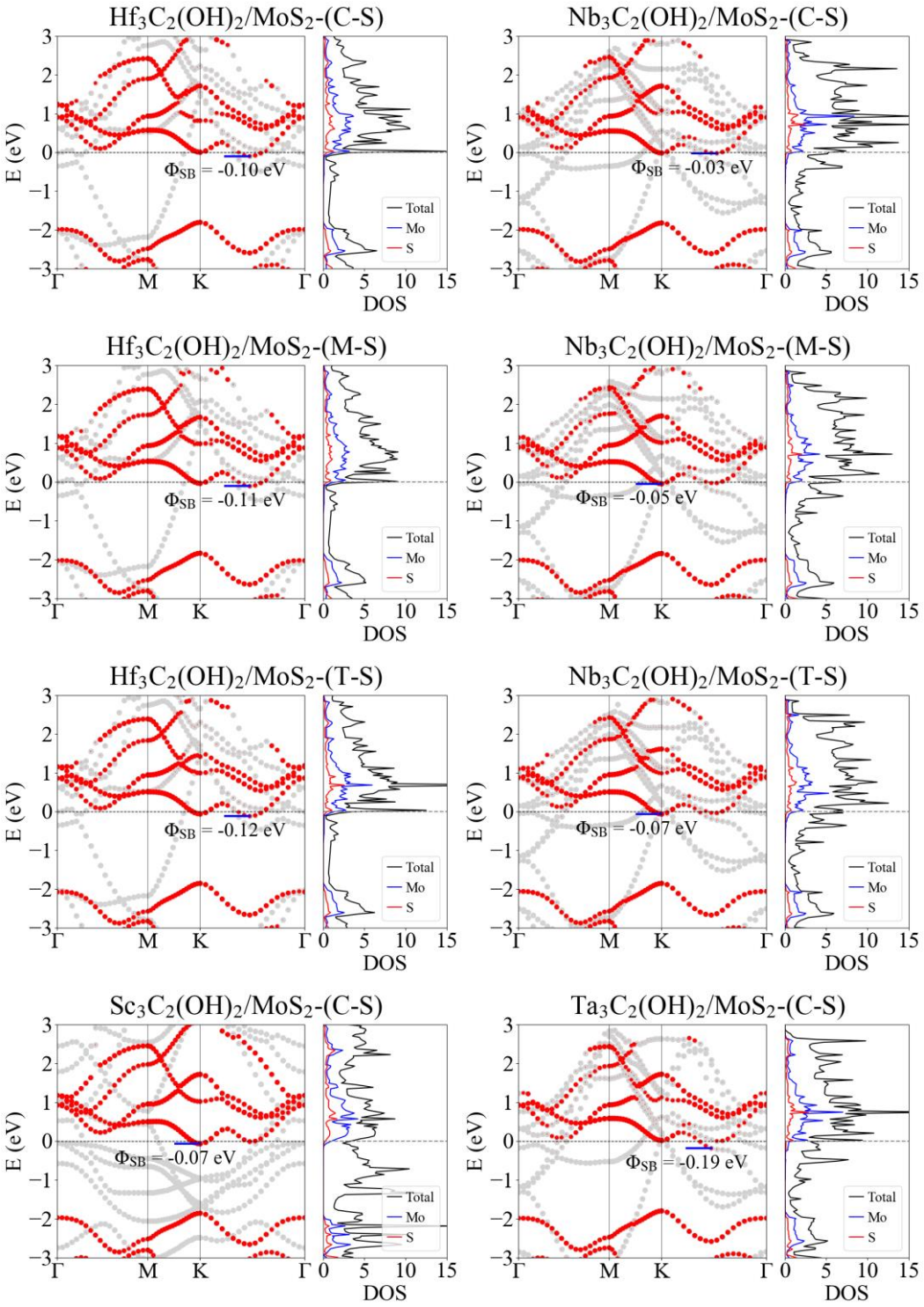

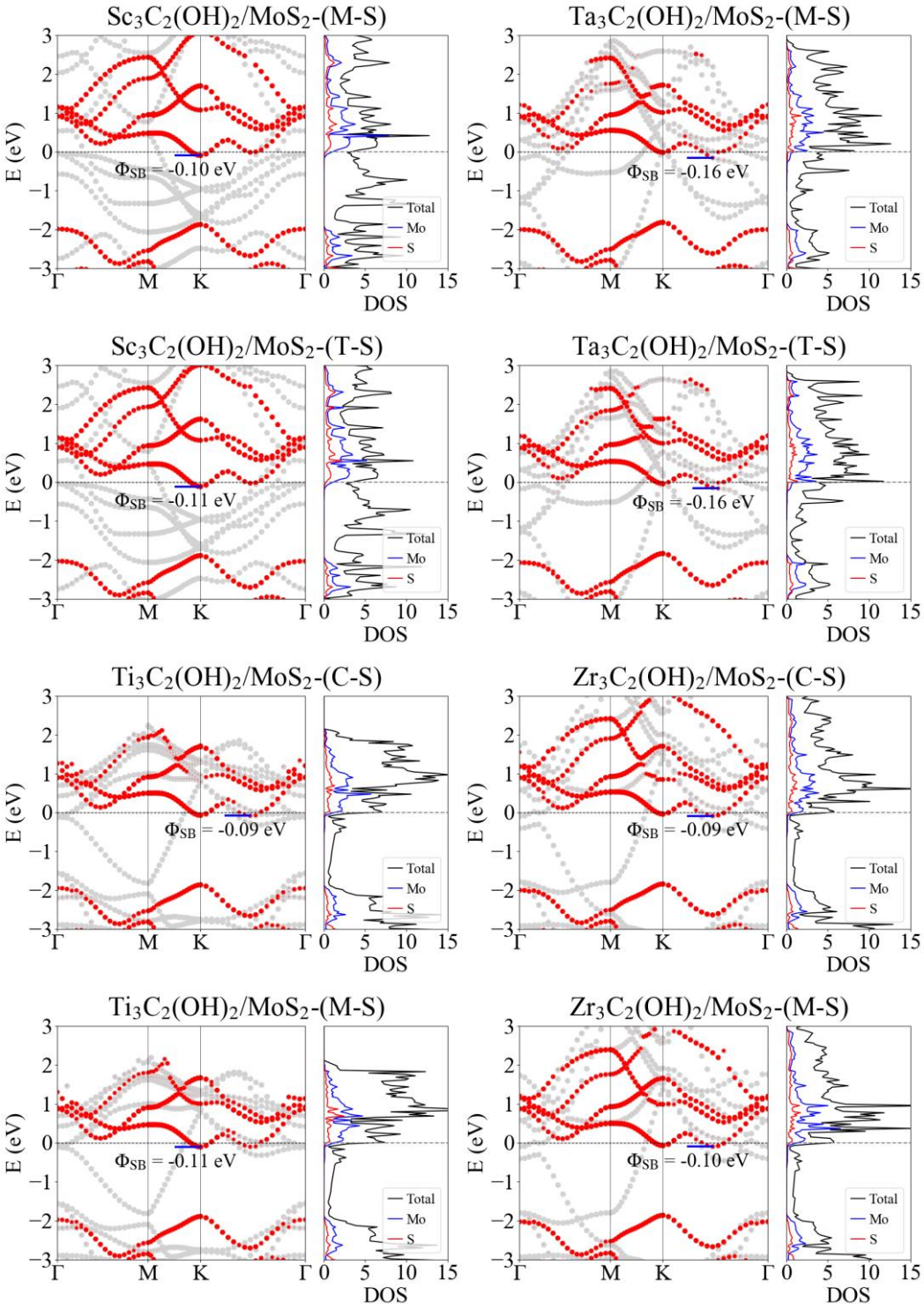
Sc3C2(OH)2/MoS2-(M-S)
ΦSB = -0.10 eV
Ta3C2(OH)2/MoS2-(M-S)
ΦSB = -0.16 eV
Sc3C2(OH)2/MoS2-(T-S)
ΦSB = -0.11 eV
Ta3C2(OH)2/MoS2-(T-S)
ΦSB = -0.16 eV
Ti3C2(OH)2/MoS2-(C-S)
ΦSB = -0.09 eV
Zr3C2(OH)2/MoS2-(C-S)
ΦSB = -0.09 eV
Ti3C2(OH)2/MoS2-(M-S)
ΦSB = -0.11 eV
Zr3C2(OH)2/MoS2-(M-S)
ΦSB = -0.10 eV
E (eV)
Γ M K Γ
DOS
Total
Mo
S

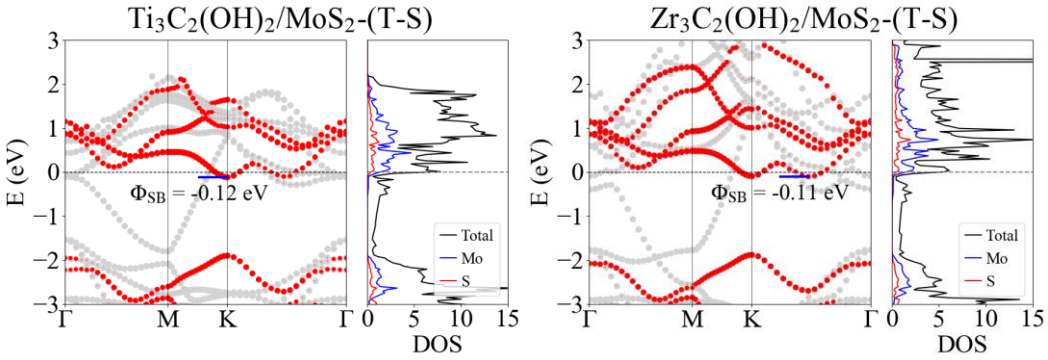
Ti3C2(OH)2/MoS2-(T-S)
Zr3C2(OH)2/MoS2-(T-S)
E (eV)
ΦSB = -0.12 eV
ΦSB = -0.11 eV
Γ
M
K
Γ
DOS
Total
Mo
S

Figure S3. The plane differential charge density plots along the z-direction under three types of stacking structures for six types of $M_3C_2(OH)_2/MoS_2$. The red areas represent charge accumulation, while the blue areas represent charge depletion.

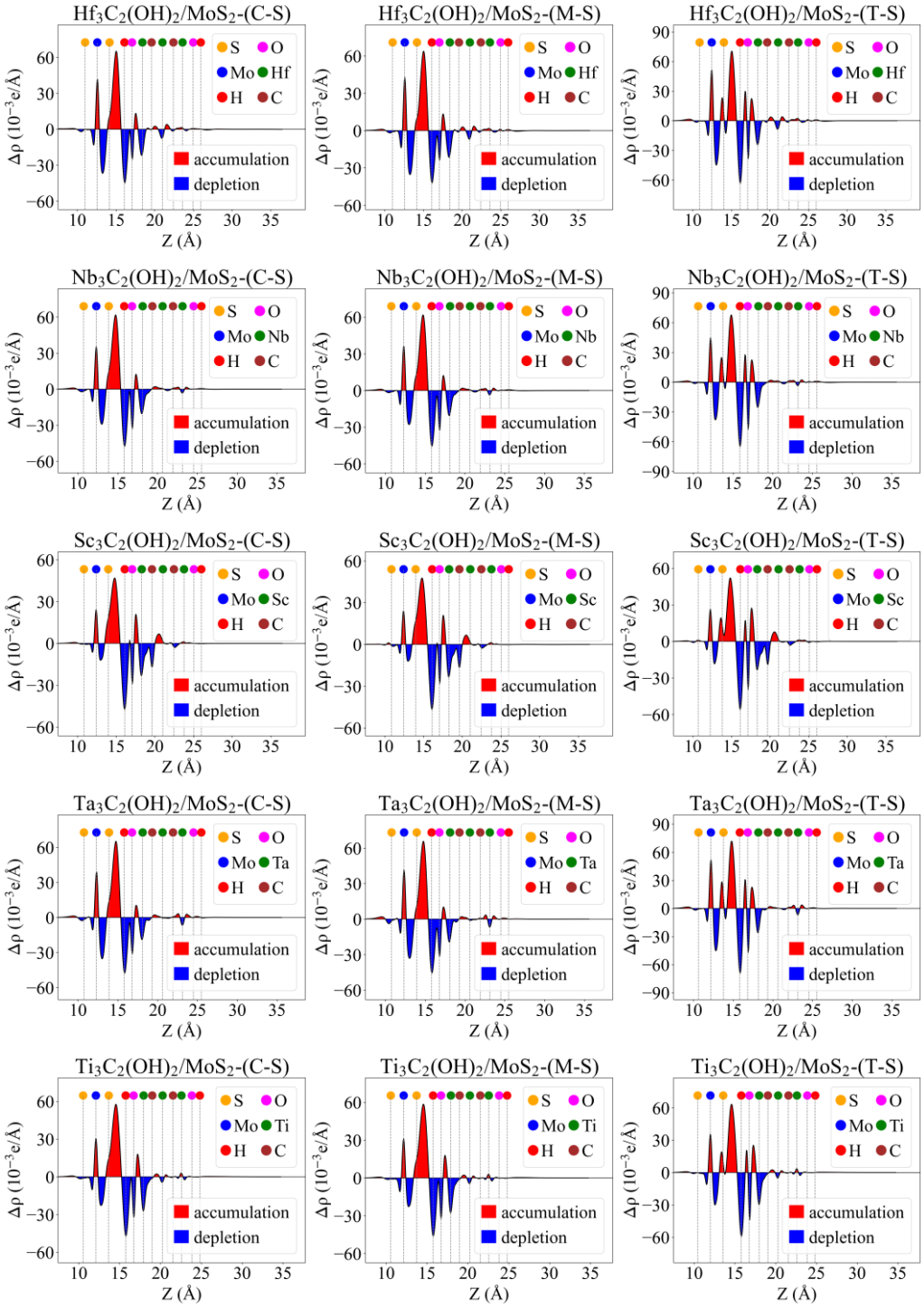

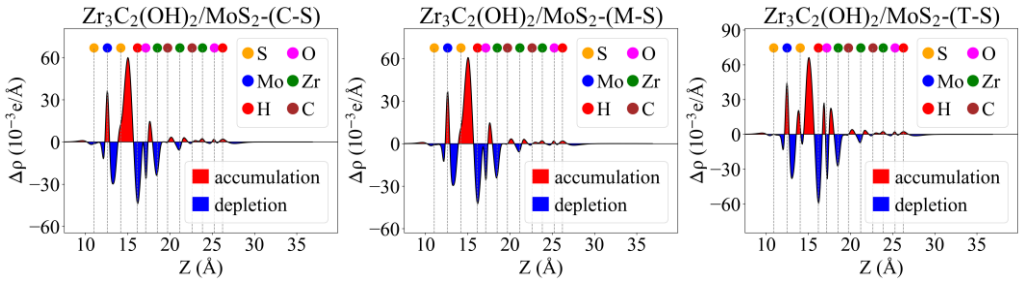
Zr3C2(OH)2/MoS2-(C-S)
Zr3C2(OH)2/MoS2-(M-S)
Zr3C2(OH)2/MoS2-(T-S)
Δρ (10−3e/Å)
Z (Å)
S
O
Mo
Zr
H
C
accumulation
depletion

Figure S4. The electrostatic potential curves along the z-direction for: (**a**) $Ta_3C_2(OH)_2$; (**b**) $Ta_3C_2O_2$; (**c**) Ta_3C_2; (**d**) $Ta_3C_2(NH)_2$. The E_f represents the Fermi level, and the center of the red dashed box corresponds to the V_{eff} point of the bottommost atom.

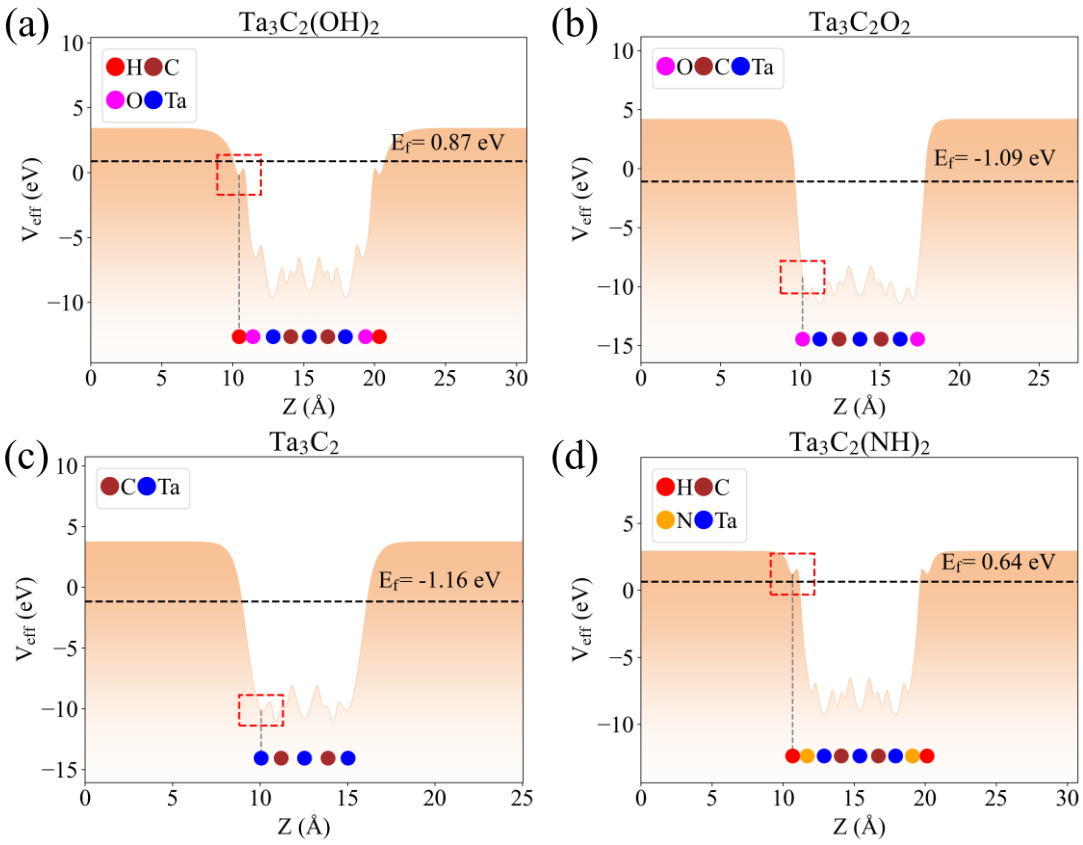

Figure S5. Projected band structures (a) with spin–orbit coupling (SOC) and (b) without SOC and electrostatic potential profiles along the z-direction (c) with SOC and (d) without SOC for the $Ta_3C_2(OH)_2/MoS_2$ heterostructure. The parameters in the projected band structures have the same meanings as in Figure S1. In the electrostatic potential profiles, E_f represents the Fermi level. W_{TB}, Φ_{TB}, and Φ_{gap} denote the tunneling barrier width, height, and the peak value, respectively. The numbers at the ends of the vertical unidirectional arrows represent the V_{eff} of the interface H atom.

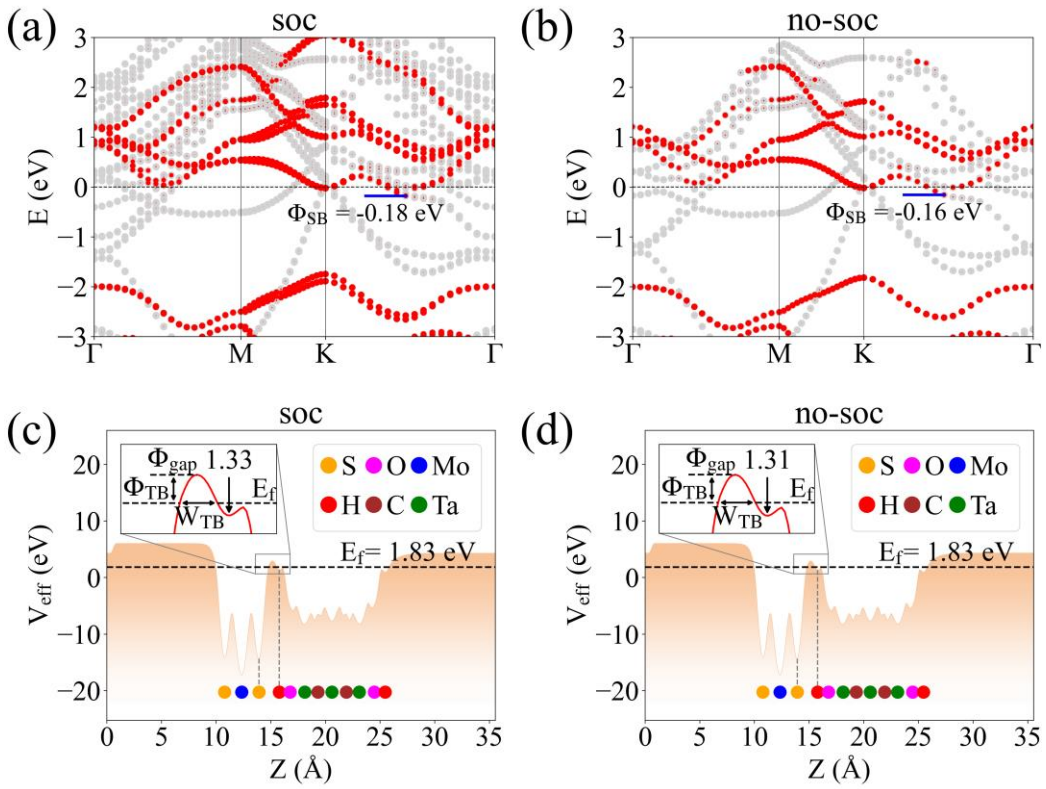

Figure S6. The tunneling probability (P_{TB}) of the $Ta_3C_2(OH)_2/MoS_2$ system based on the M-S model as a function of the interlayer spacing (*d*). In the legend, 0 is the reference object (*d* is 1.87 Å), and the others are based on increasing and decreasing d from this point.

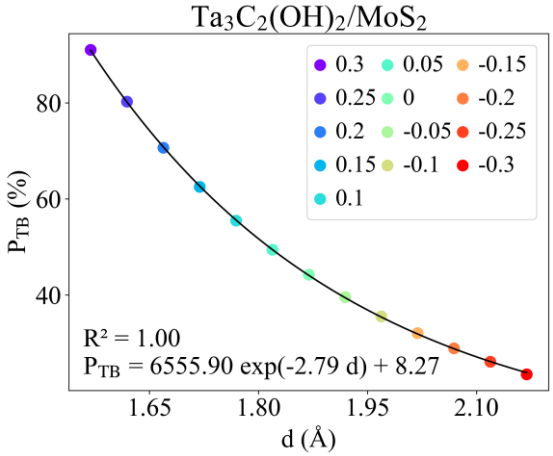

Figure S7. The electrostatic potential curves along the z-direction for 6 types of $M_3C_2(NH)_2/MoS_2$ and 6 types of $M_3N_2(NH)_2/MoS_2$ heterostructures. The corresponding parameter definitions are the same as those in Figure S5.

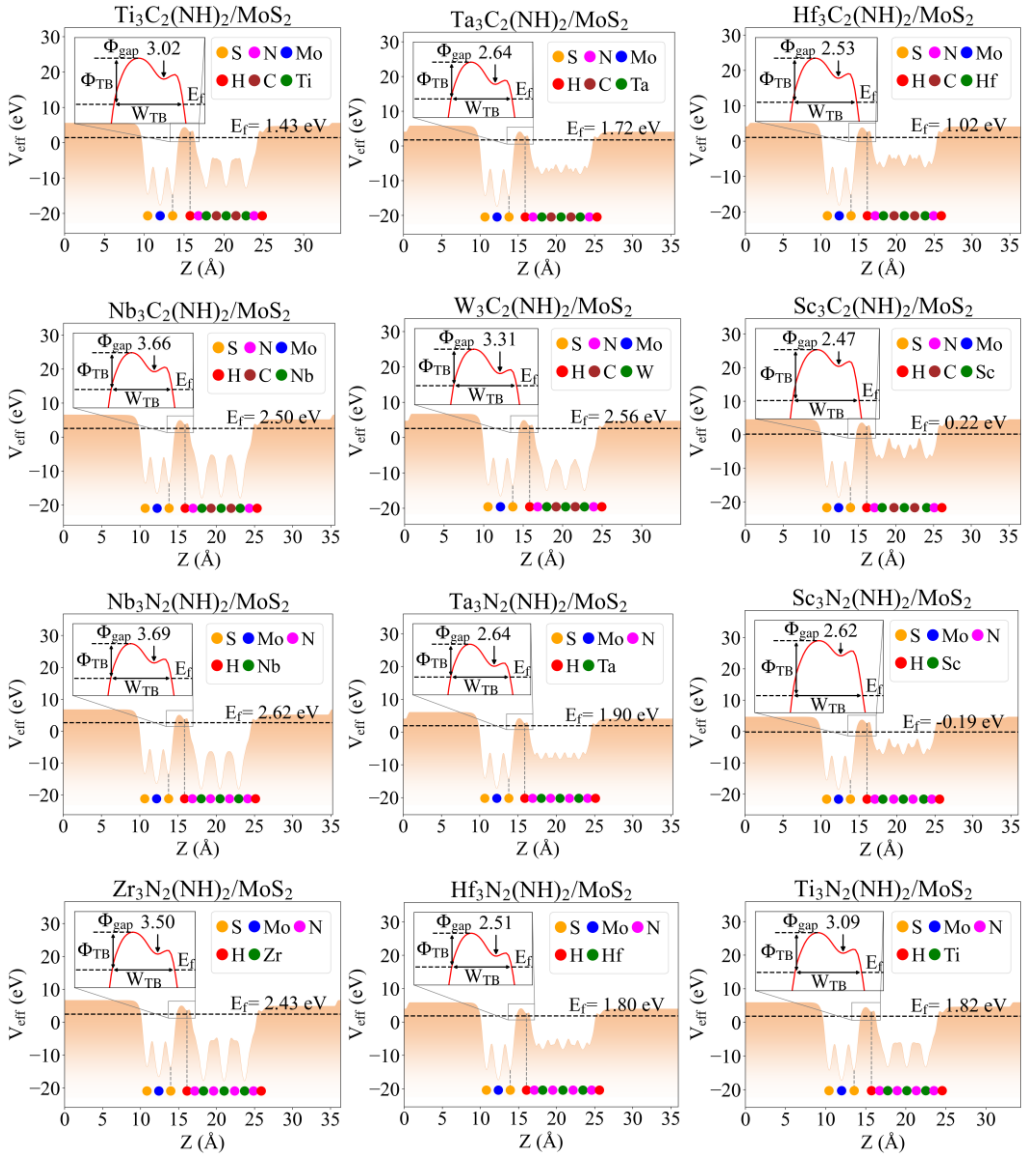

Figure S8. Relationship diagrams of tunneling probability versus (**a**) interlayer spacing and (**b**) binding energy for $M_3X_2(OH)_2/MoS_2$(X=C/N) heterostructures.

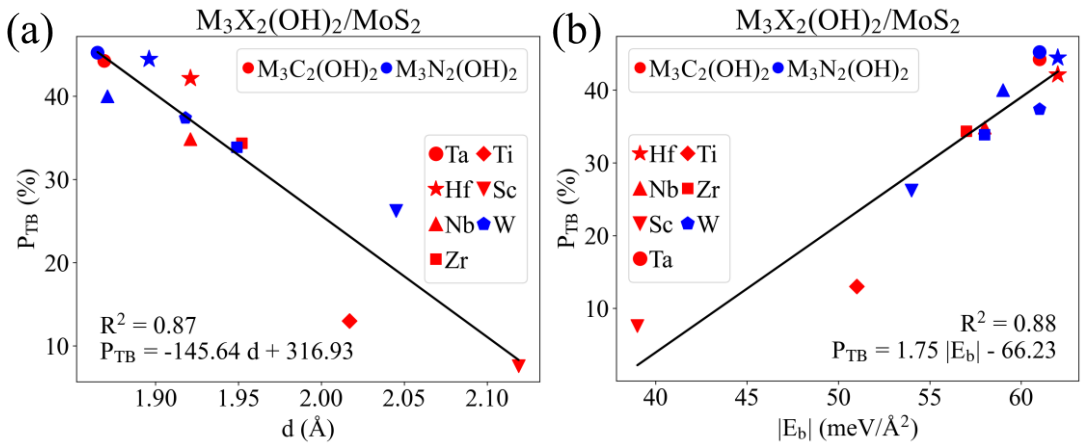

Figure S9. The electrostatic potential curves along the z-direction for the $Ti_3C_2(OH)_2/MoS_2$ heterostructure under biaxial strain ranging from -2% to 2%. The corresponding parameter definitions are the same as those in Figure S5.

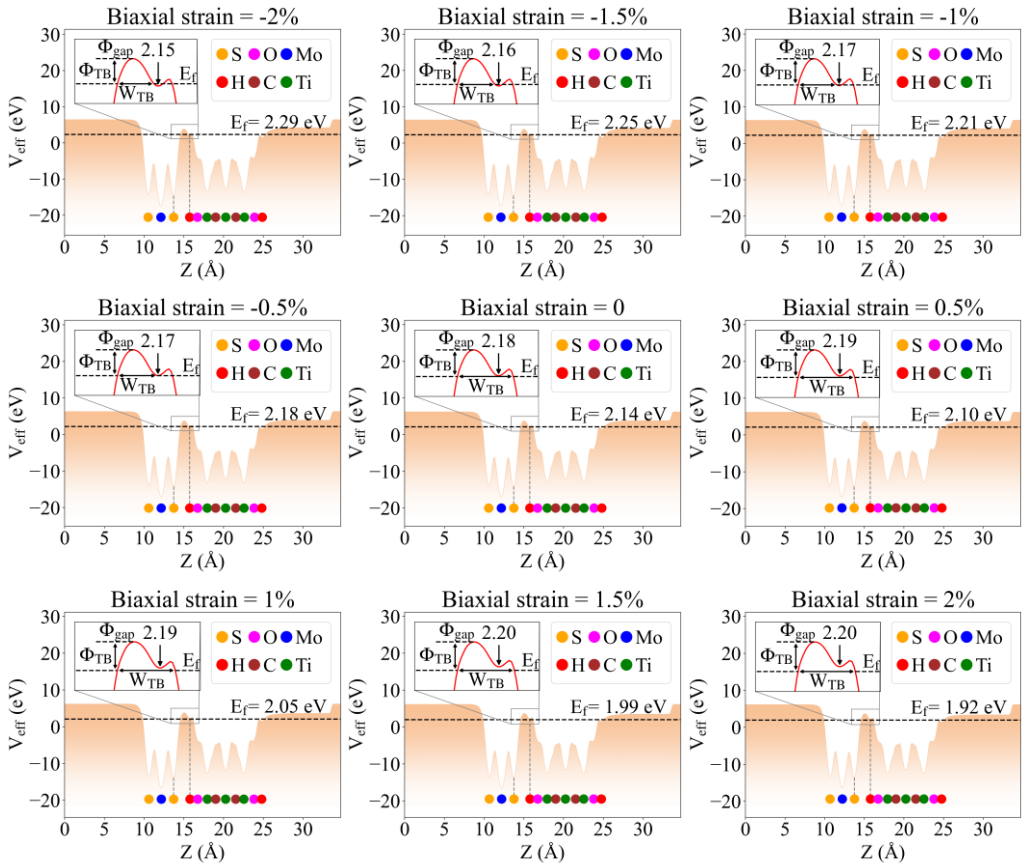

Figure S10. (**a**) Phonon spectrum of the $Ti_3C_2(OH)_2/MoS_2$ heterostructure under -2% biaxial strain, and (**b**) temperature and (**c**) energy change diagrams during 10 ps of molecular dynamics simulation at 300 K.

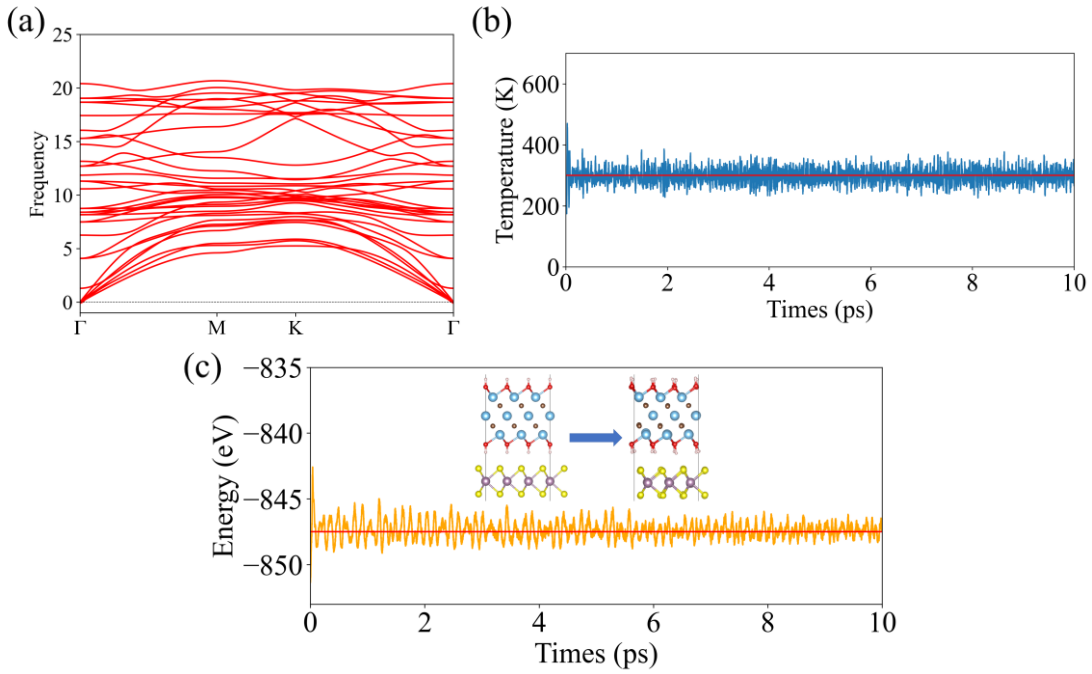

Figure S11. The variation of the band gap (gap) of MoS_2 and the Schottky barrier (Φ_n) at the $Ti_3C_2(OH)_2/MoS_2$ heterostructure under biaxial strain. The value of gap_0 is 1.76 eV, corresponding to the orange dashed line, and the purple dashed line corresponds to "$\Phi_n = 0$".

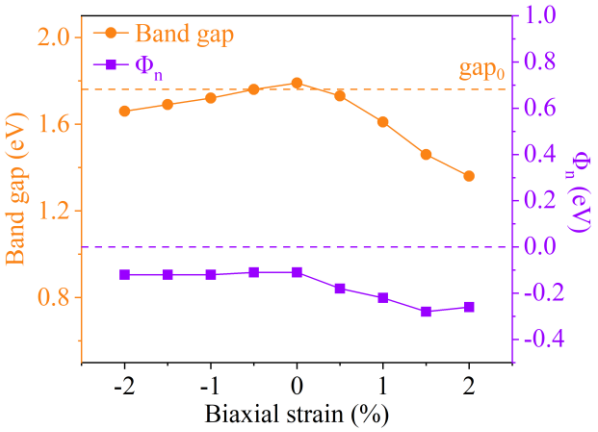

Table S1. Mismatch degrees (Mismatch) of six types of $M_3C_2(OH)_2/MoS_2$ heterostructures.

$M_3C_2(OH)_2/MoS_2$	Ti	Nb	Ta	Hf	Zr	Sc
Mismatch(%)	3.21	1.92	2.16	3.57	4.85	2.85

Table S2. Binding energy (E_b) and Schottky barrier (Φ_{SB}) for the three models of six types of $M_3C_2(OH)_2/MoS_2$ heterostructures.

MXene/MoS_2	**Model**	E_b **(meV/Å^2)**	Φ_{SB} **(eV)**
	C-S	-61	-0.10
$Hf_3C_2(OH)_2$	M-S	-62	-0.11
	T-S	-65	-0.12
	C-S	-57	-0.03
$Nb_3C_2(OH)_2$	M-S	-58	-0.05
	T-S	-60	-0.07
	C-S	-61	-0.19
$Ta_3C_2(OH)_2$	M-S	-61	-0.16
	T-S	-65	-0.16
	C-S	-50	-0.09
$Ti_3C_2(OH)_2$	M-S	-51	-0.11
	T-S	-53	-0.12
	C-S	-56	-0.09
$Zr_3C_2(OH)_2$	M-S	-57	-0.10
	T-S	-60	-0.11
	C-S	-38	-0.07
$Sc_3C_2(OH)_2$	M-S	-39	-0.10
	T-S	-39	-0.11

Table S3. Comparative electronic properties of $Ta_3C_2(OH)_2/MoS_2$ heterostructure with and without spin-orbit coupling (SOC): tunneling barrier height (Φ_{TB}), width (W_{TB}), probability (P_{TB}), impedance (ρ_T), effective potential at interface H (V_H), and Fermi level (E_f).

	W_{TB}(Å)	Φ_{TB}(eV)	P_{TB}(%)	ρ_T (e^{-9} Ωcm^2)	V_H(eV)	E_f(eV)
SOC	0.77	1.11	43.66	0.035	1.33	1.83
no-SOC	0.76	1.09	44.24	0.035	1.31	1.83

Table S4. The tunneling barrier width (W_{TB}), height (Φ_{TB}), tunneling probability (P_{TB}), tunneling impedance (ρ_T), and interlayer spacing (d) after structural optimization for three models of $M_3C_2(OH)_2/MoS_2$ heterostructures.

MXene/MoS_2	**model**	**W_{TB}(Å)**	**Φ_{TB}(eV)**	**P_{TB}(%)**	**ρ_T(10^{-9} Ω cm^2)**	***d*(Å)**
	C-S	0.80	1.20	40.61	0.038	1.89
$Ta_3C_2(OH)_2$	M-S	0.76	1.09	44.24	0.035	1.87
	T-S	0.98	1.59	28.20	0.058	2.06
	C-S	0.80	1.17	41.00	0.038	1.92
$Hf_3C_2(OH)_2$	M-S	0.79	1.14	42.15	0.037	1.92
	T-S	1.00	1.61	27.26	0.061	2.10
	C-S	0.93	1.40	32.61	0.051	1.94
$Nb_3C_2(OH)_2$	M-S	0.89	1.32	34.86	0.047	1.92
	T-S	1.11	1.79	21.77	0.080	2.12
	C-S	0.95	1.43	31.21	0.054	1.99
$Zr_3C_2(OH)_2$	M-S	0.90	1.33	34.35	0.048	1.95
	T-S	1.13	1.80	21.22	0.084	2.15
	C-S	1.62	1.72	11.38	4.31	2.06
$Ti_3C_2(OH)_2$	M-S	1.57	1.61	13.01	15.54	2.02
	T-S	1.80	2.03	7.24	2.31	2.22
	C-S	1.76	2.09	7.42	2.24	2.13
$Sc_3C_2(OH)_2$	M-S	1.75	2.07	7.59	2.26	2.12
	T-S	1.96	2.41	4.38	2.53	2.32

Table S5. The mismatch, Φ_{SB}, and E_b of $M_3X_2T_2/MoS_2$(X=N, T=OH/NH; X=C, T=NH) heterostructures.

MXene/MoS_2	**Mismatch(%)**	**Φ_{SB} (eV)**	**E_b (meV/Å^2)**
$Hf_3N_2(OH)_2$	0.32	-0.09	-62
$Nb_3N_2(OH)_2$	2.50	-0.02	-59
$Sc_3N_2(OH)_2$	1.06	-0.09	-54
$Ta_3N_2(OH)_2$	3.26	-0.04	-61
$W_3N_2(OH)_2$	1.85	-0.06	-61
$Zr_3N_2(OH)_2$	1.95	-0.06	-58
$Hf_3C_2(NH)_2$	3.77	-0.06	-32
$Nb_3C_2(NH)_2$	0.21	0.01	-35
$Sc_3C_2(NH)_2$	4.94	0.19	-27
$Ta_3C_2(NH)_2$	0.22	-0.09	-37
$Ti_3C_2(NH)_2$	3.72	-0.02	-29
$W_3C_2(NH)_2$	2.60	-0.07	-39
$Hf_3N_2(NH)_2$	2.49	-0.13	-38
$Nb_3N_2(NH)_2$	1.56	-0.03	-37
$Sc_3N_2(NH)_2$	2.57	0.79	-27
$Ta_3N_2(NH)_2$	1.28	-0.05	-40
$Ti_3N_2(NH)_2$	4.83	-0.07	-32
$Zr_3N_2(NH)_2$	3.83	-0.10	-35

Table S6. The W_{TB}, Φ_{TB}, P_{TB}, ρ_T, and d for $M_3X_2T_2/MoS_2$ heterostructures.

MXene/MoS_2	**W_{TB}(Å)**	**Φ_{TB}(eV)**	**P_{TB}(%)**	**ρ_T(10^{-9} Ω cm^2)**	***d*(Å)**
$Ta_3N_2(OH)_2$	0.74	1.08	45.24	0.033	1.87
$Hf_3N_2(OH)_2$	0.76	1.09	44.47	0.035	1.90
$Nb_3N_2(OH)_2$	0.82	1.19	40.01	0.040	1.87
$W_3N_2(OH)_2$	0.86	1.26	37.39	0.043	1.92
$Zr_3N_2(OH)_2$	0.90	1.36	33.86	0.048	1.95
$Sc_3N_2(OH)_2$	1.04	1.57	26.22	0.067	2.05
$W_3C_2(NH)_2$	1.77	2.30	6.36	2.13	2.13
$Ta_3C_2(NH)_2$	1.78	2.35	6.14	2.11	2.11
$Nb_3C_2(NH)_2$	1.78	2.41	5.89	2.10	2.10
$Hf_3C_2(NH)_2$	1.89	2.78	4.00	2.37	2.17
$Ti_3C_2(NH)_2$	1.94	2.90	3.40	2.59	2.21
$Sc_3C_2(NH)_2$	1.97	3.36	2.49	2.97	2.17
$Ta_3N_2(NH)_2$	1.72	2.23	7.16	2.11	2.08
$Hf_3N_2(NH)_2$	1.75	2.25	6.80	2.12	2.12
$Nb_3N_2(NH)_2$	1.76	2.42	6.03	2.07	2.08
$Zr_3N_2(NH)_2$	1.83	2.55	5.00	2.19	2.15
$Ti_3N_2(NH)_2$	1.85	2.63	4.62	2.24	2.16
$Sc_3N_2(NH)_2$	2.06	3.90	1.56	4.07	2.20

Table S7. The W_{TB}, Φ_{TB}, P_{TB}, ρ_T, the MoS_2 bandgap (gap), Φ_{SB}, d and E_b of $Ti_3C_2(OH)_2/MoS_2$ heterostructures under a biaxial strain range from -2% to 2%.

Biaxial strain (%)	**W_{TB} (Å)**	**Φ_{TB} (eV)**	**P_{TB} (%)**	**ρ_T (10^{-9} Ω cm^2)**	**gap (eV)**	**Φ_{SB} (eV)**	***d* (Å)**	**E_b (meV/ Å^2)**
-2	1.02	1.55	27.10	0.064	1.66	-0.12	2.02	-54.5
-1.5	1.06	1.59	25.55	0.069	1.69	-0.12	2.03	-53.6
-1	1.08	1.60	24.61	0.073	1.72	-0.12	2.02	-52.6
-0.5	1.11	1.57	24.10	0.077	1.76	-0.11	2.00	-51.7
0	1.57	1.61	13.01	15.54	1.79	-0.11	2.02	-51.0
0.5	1.59	1.66	12.20	6.51	1.73	-0.18	2.03	-50.4
1	1.62	1.73	11.27	4.12	1.61	-0.22	2.05	-50.0
1.5	1.60	1.72	11.73	4.92	1.46	-0.28	2.01	-49.8
2	1.61	1.78	11.13	3.85	1.36	-0.26	2.01	-49.7